Journal of Ultrafine Grained and Nanostructured Materials
https://jufgnsm.ut.ac.ir
Vol. 54, No.1, June 2021, pp. 29-39
Print ISSN: 2423-6845 Online ISSN: 2423-6837
DOI: 10.22059/jufgnsm.2021.01.03

Effect of Zener-Hollomon Parameter on Microstructure of Aluminum Based Nanocomposite Layers Produced by Friction Stir Processing

Aziz Shafiei-Zarghani*[*,1], Abolfazl Najafi[1], Seyed Farshid Kashani-Bozorg[2], Abbas Zarei-Hanzaki[3]

[1]Department of Materials Science and Engineering, School of Engineering, Shiraz University, Shiraz, Iran.
[2]Center of Excellence for Surface Engineering and Corrosion Protection of Industries, College of Engineering, School of Metallurgy and Materials Engineering, University of Tehran, Tehran, Iran.
[3]Hot Deformation and Thermomechanical Processing Laboratory of High Performance Engineering Materials, School of Metallurgy and Materials Engineering, College of Engineering, University of Tehran, Tehran, Iran.

Recieved: 28 January 2021; Accepted: 29 April 2021
** Corresponding author email: ashafiei@shirazu.ac.ir*

ABSTRACT

For more than a decade, there has been considerable interest in the fabrication of metal matrix composites by employing Friction Stir Processing (FSP). In this study a new model based on Zener-Hollomon (Z) parameter has been developed, which is believed to be the first of its kind, to accurately predict microstructural characteristics of Al-based composites Additionally, the processing window of composite fabrication determined and revealed that sound samples achieve within the range of 2.42 to 24.61 rev/mm for the ratio of rotation speed to travel speed (ω/v). Recording the peak temperatures during processing beside the optical and Scanning Electron Microscopic (SEM) studies showed that increasing the number of FSP passes and the ratio of ω/v have a remarkable influence on bolstering the role of nanoparticles in grain refinement. Results also indicated that the mean grain size of FSPed samples and matrix of nanocomposites decreases with an increase in the Z parameter. Finally, particular equations for various numbers of passes developed, which make a correlation between the grain size of Al-based composites and the FSP parameters via Z parameter.

Keywords: *Metal Matrix Composites, Zener-Hollomon Parameter, Friction Stir Processing, Aluminum.*

1. Introduction

Over past few years, aluminum matrix composites (AMCs) have become intriguing to many researchers due to their high specific strength and young modulus, good resistance to corrosion, creep, fatigue, and wear and their high thermal conductivity. Aluminum based composites are typically utilized in automotive, construction and aerospace industries. Additionally, AMCs reinforced with ceramic particles are widely used in these industries due to their unique properties and high particular strength. Recently, several techniques such as laser beam radiation [1] electron beam radiation [2] and plasma spray [3] have been developed in order to fabricate Al based surface composite layers. Since these high energy processes are performed at high temperature and in liquid phase, during these processes some reactions may take place that lead to formation of brittle phases. Another challenge is that parameters

of the process must be chosen very accurately in order to achieve desirable microstructure. Moreover, there are limitations related to the size of reinforcing particles. The problem is that in fusion processes, reinforcing particles must be wetted by liquid phase and the smaller the particles, the more difficult the wettability will be. While one of the most effective factors on strength and hardness of composites is the size of reinforcing particles. In a way, that the smaller particles will cause more strengthening and hardening of composites. Therefore, if the process of creating the surface composite layers can be implemented at lower temperature in solid state, the problem can be overcome. Friction Stir Processing (FSP) is a solid state processing technique, which can avoid the inherent disadvantages of liquid based processes. A rotating tool with specially designed pin and shoulder is plunged into a plate and then traverses along the scheduled line accompanied with severe plastic deformation. FSP is a versatile technique, which can be utilized for production of surface layers with the required functional properties and it enables us to fabricate composite materials by introducing second phase reinforcement [4,5]. Besides, FSP provides microstructural refinement and it can locally eliminate possible imperfections, which results in improving strength and ductility. FSP also can increase the corrosion and fatigue resistance, and enhance formability [6-8].

In the case of composites grain size and strengthening role of reinforcement particles, one of the most determinant microstructural factors is distance of reinforcement particles (L) which can be estimated by Eq. 1 [9].

$$L = \left(\frac{d}{2}\right)\left(\frac{2\pi}{3V_f}\right)^{1/2} \quad (1)$$

Where d is the average diameter of reinforcements, and V_f is the volume fraction of them. For example, in a hypothetical Al-particulate composite containing 20% volume fraction of reinforcements with an average size of 20 μm, the value of L is about to 32 μm. While by using the nano-sized particles (e.g. 10-50 nm), with addition far less percent of them, the distance of particles equals to 100-1000 nm. In our previous work[5];the effects of volume fraction and size of reinforcement particles were studied on grain size of Al matrix by employing zener limiting equation comprehensively and it is considered that the limiting effect by nano-sized particles retarded the grain growth of Al matrix which resulted in enhancing the mechanical properties. Accordingly, this process enables us to fabricate ultrafine grain matrix composites. As an example, Rajeshkumar et al. [10] employed a single pass of FSP to refine the grains of a preprepared Al-graphite composite. The grain size of the composite was reduced significantly to ultrafine range and as a result of uniform dispersion of fine graphite particles, which was achieved due to strong stirring action of rotating tool, the samples exhibited superior hardness. In another work, You et al. [11] produced Al matrix composites reinforced with nano-sized Al_2O_3 particles from Al-SiO_2 powder mixture by using FSP. Microstructural examination revealed that the Al_2O_3 particles present mainly in the form of clusters of nano-sized particles with fine dispersion in an ultrafine-grained Al matrix. Accordingly, composites exhibited sustainable tensile strength and ductility.

One of the most necessary aspects of every process should be the ability of modeling the process variables with a formula in order to predict the result prior to operating the process. The temperature and strain rate dependence on plastic deformation can be analyzed using the Zener-Hollomon (Z) parameter. The Z parameter was originally proposed to describe the combined effect of strain rate and temperature of thermomechanical process on achieved flow stress of metals at or below room temperature. For instance, Moghadam et al. [12] conducted a study to investigate microstructural, mechanical and texture evolutions of a 7075 aluminum alloy at the early stage of severe plastic deformation during three different process under predetermined thermomechanical condition based on the Z parameter values. In another work, Lapin and co-authors [13] investigated the hot deformation behavior and microstructure of TiAl based alloy reinforced with carbide particles. They concluded that the size of recrystallized grains increases with decreasing Z parameter. In addition, Jain et al. [14] has characterized the Al5083-CNTs/SiC composites developed via FSP and demonstrated that Zener-Hollomon is the dominant restoration mechanism. Moreover, Abbasi et al. [15] has subject Al powder metallurgy to FSP and results illustrated that due to increase of Z parameter the average grain size decreased. There are also a few more investigations on the effects of Z parameter on microstructure of FSPed or FSWed steels [16,17], copper [18] and magnesium [19,20] alloys. However, literature

survey depicts that to date there has not been an adequate analytical model based on Z parameter to predict the microstructural characteristics of composite materials produced by FSP. Accordingly, this study aims to provide a simple equation for predicting the matrix grain size of Al-based composites using Z parameter, which represents process parameters of FSP. For this purpose, different samples in two groups -with and without reinforcements- were subjected to FSP under a wide variety of parameters including rotation and travel speeds and number of passes. Then, after obtaining the processing window, the model was developed. This model can be used with caution for Al composites fabricated by 1 to 4 FSP passes. To apply this model it is required to consider some parameters including tool's geometry and particle size of reinforcements.

2. Experimental procedures

In this study, Al 6082 alloy plates with chemical composition which is given in Table 1 and dimensions of 200×75×7 mm were used as substrate. In order to incorporate Al_2O_3 powders, a groove with depth and width of 4 and 1 mm, respectively, was machined on the surface in centerline and in longitudinal direction. Then, to remove all surface contaminations, prepared workpieces were placed in solution of acetone and alcohol and cleaned in an ultrasonic bath. Alpha type Al_2O_3 powders with purity of 99.8% and average particle size of 50 nm were dried in furnace at 200 °C for 30 minutes and placed into the grooves. FSP tool was built from hot-work steel H13 and undergone hardening heat treatment. Hardness of the tool were varied between 58 and 61 HRC. Shoulder and pin of the tool were designed with diameters of 16 and 5 mm, respectively, and pin height was 4 mm. FSP was performed by utilizing a conventional milling machine with stationary top part and movable desk. Depth penetration of the shoulder was fixed to 0.2 mm and tilt angle of tool axes with normal axes of workpieces was entered the sheet with 3°. To preclude the spreading out of powders during the FSP, a pin-less tool was employed to seal the groove prior FSP. Surface composite layers were fabricated by one to four FSP passes with rotation speeds of 630, 800, 1000, 1250 and 1600 rpm and travel speeds of 35 and 560 mm/min. Moreover, in order to reveal the influence of Al_2O_3 nano particles on evolution of microstructure, some aluminum sheets encountered FSP without Al_2O_3 powder. After each pass and before conducting the next pass, specimens were cooled down to room temperature. In order to determine the peak temperature during process, a K type thermocouple was placed below the substrate in the middle of the FSP track, where metallographic samples were cut from.

Transverse and longitudinal sections of the specimens were mounted for microstructural studies and then grounded with SiC papers and polished with diamond paste. After that they were electropolished according to conditions illustrated in Table 2. Temperature of electropolish solution was kept constant by placing it's container in mixture of dried ice and methanol. Prepared specimens were examined via optical microscope Olympus BX60M. In addition, in order to evaluate the microstructure and grain boundaries of the polished samples, the composite layers were examined before and after etching using a CamScan MV2300 Scanning Electron Microscope (SEM). Etching process was carefully performed in accordance with ASM Handbook with a solution by composition of 42.5 ml H_2O, 30 ml HCL, 40 ml HNO_3 and 5.2 ml HF.

3. Results and Discussion

3.1. Investigation of defects in surface composite layers

Visual and microscopic examination of specimens revealed that there are generally two kinds of imperfections in specimens, which are shown in Fig. 1. In Fig. 1(a) blistering on the surface, which is attributed to excessive process heat input is illustrated. Existence of porosity and

Table 1- Chemical composition of as received Al 6082

Element	Si	Mg	Mn	Fe	Cr	Cu	Zn	Al
Weight Percentage	1.2	0.78	0.5	0.33	0.14	0.08	0.05	balance

Table 2- Electropolishing solution and parameters of FSPed samples and surface composite layers

Solution		Flow	Time	Voltage	Temperature
Ethyl Alcohol Absulute	Prechloric Acid (60%)	(A/mm^2)	(s)	(V)	(°C)
550 ml	110 ml	0.03	60	30	-80

cavities at the bottom of stirred zone and its border with base metal is shown in Fig. 1(b), which is related to inadequate heat input and material flow. Increasing the ratio of ω/ν caused an increase in the heat input, which is a consequent of intensifying the friction between tool and workpiece as well as the amount of plastic deformation. This expression is demonstrated in Fig. 2 as the relationship between processing speeds and heat input in terms of experimental recorded peak temperature.

With decreasing the ratio of ω/ν, some cavities were formed at the bottom of stirred zone and its interface with the substrate, which is attributed to low heat input and insufficient material flow around the pin. Formation of these cavities led to accumulation and trapping of Al_2O_3 reinforcements and consequently nonuniform distribution of these ceramic particles. While, at constant rotation speed (e.g. 630 rpm) with decreasing travel speed (from 530 mm/min to 35 mm/min) cavities disappeared and defect free composites were achieved. The recorded results of temperature peaks also indicate the same trend. As it can be observed in Fig. 2, at constant travelling speed, peak temperature increased with increasing rotation speed; besides, at constant rotation speed, it decreased with increasing travel speed. The maximum peak temperature, which is related to ω of 1600 rpm and ν of 35 mm/min was 552 °C. While, the lowest peak temperature is 365 °C for ω of 630 rpm and ν of 530 mm/min. Since the liquidus and solidus temperatures of the base alloy are 582 °C and 682 °C, respectively, it can be concluded that no melting was occurred during the FSP and the whole process was performed in solid state.

The amount of generated heat (q) during the FSP can be estimated by the following equation [21]:

$$q = \frac{4}{3}\pi^2 \mu P \omega R^3 \quad (2)$$

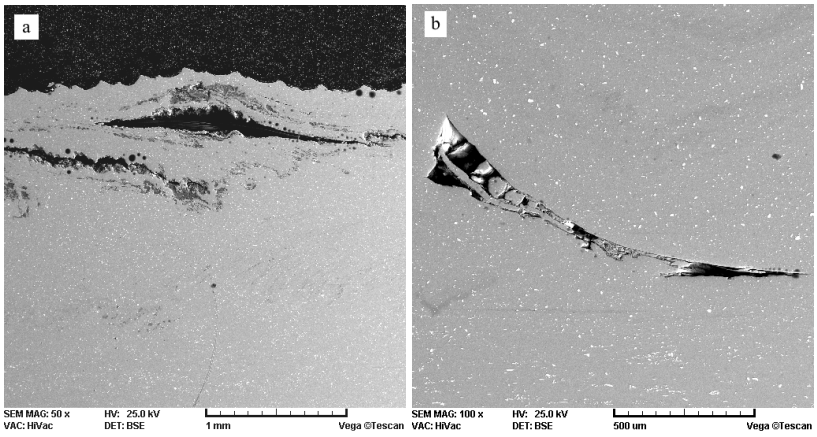

Fig. 1- SEM phographs of a) longitudinal section of surface composite layer fabricated at rotation speed of 1600 rpm and travel speed of 35 mm/min b) traversal section of surface composite layers at rotation speed of 630 rpm and travel speed of 530 mm/min.

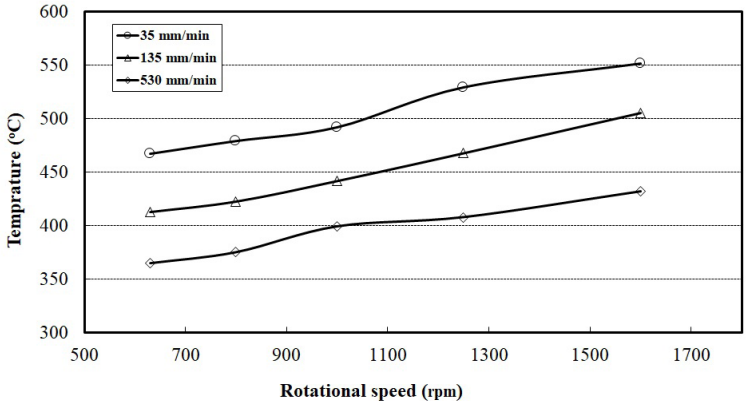

Fig. 2- Variation of peak temperature during FSP at different rotation and travel speeds

Where μ is friction coefficient, P is vertical pressure, and R is shoulder diameter. From Eq. 2, heat input per unit length of Friction Stir Processed (FSPed) surface can be written in terms of FSP variables as below:

$$Q = \frac{\alpha q}{\nu} = \frac{3}{4}\pi^2 \frac{\alpha \mu P \omega R^3}{\nu} \quad (3)$$

where α is heat input efficiency, α and μ are considered constant in all parameters. Eq. 3 can be simplified as:

$$Q \propto \frac{\omega}{\nu} \quad (4)$$

According to Eq. 4, if the ω/ν ratio is greater than a certain level, the amount of heat input per unit length would exceed the critical value, which may result in blistering. On the other hand, if this ratio is less than desired limit, the amount of heat input would descend too much and consequently some cavities form at bottom part of stirred zone. The lower and higher critical values for this ratio are 2.42 ($\frac{800\ rpm}{330\ mm/min}$) and 24.61 ($\frac{1600\ rpm}{65\ mm/min}$), respectively. Processing window and status of created defects in surface composite layers at different variables along with the ω/ν ratio for each sample is demonstrated in Fig. 3.

3.2. Microstructure

Optical macrographs of cross section of surface composite layers fabricated with various variables are shown in Fig 4. In samples fabricated with travel speed of 135 mm/min, it can be observed that depth and width of stirred zone were increased with increasing rotation speed. Same trend is obvious in travel speed of 330 mm/min. In addition, it is clear that at all rotation speeds with increasing ν, both depth and width of the stirred zone were decreased. These observations are also depicted in Fig. 5. According to this figure, it can be concluded that area of stirred zone increased with increasing ω at constant ν, and with decreasing ν at constant ω.

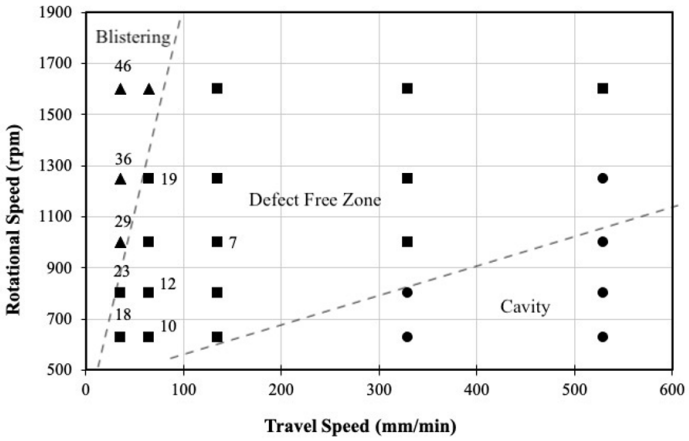

Fig. 3- Status of presented defects at various parameter of FSP and fraction of rotation speed to travel speed.

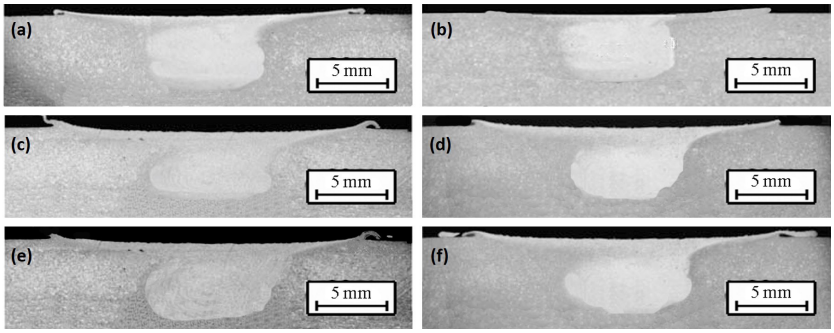

Fig. 4- Macrographs of cross section of surface composite layers at a) rotation speed of 1000 rpm and travel speed of 135 mm/min b) rotation speed of 1000 rpm and travel speed of 330 mm/min c) rotation speed of 1250 rpm and travel speed of 135 mm/min d) rotation speed of 1250 rpm and travel speed of 330 mm/min e) rotation speed of 1600 rpm and travel speed of 135 mm/min f) rotation speed of 1600 rpm and travel speed of 330 rpm.

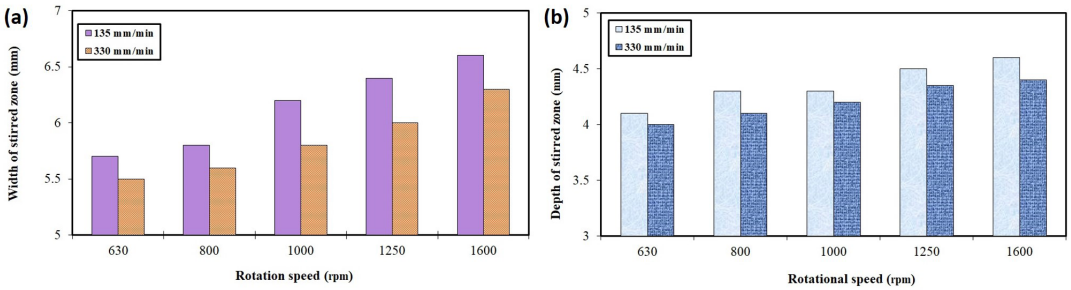

Fig. 5- Variation of a) maximum width and b) depth of stirred zone by rotation speed at travel speeds of 135 mm/min and 330 mm/min.

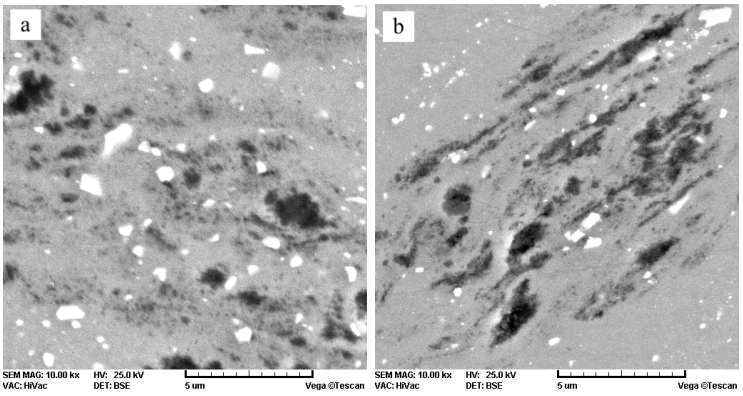

Fig. 6- SEM images of distribution of AL_2O_3 particles in surface composite layers with one pass of FSP at rotation speed of 1000 rpm and travel speed of a) 135 mm/min b) 330 mm/min.

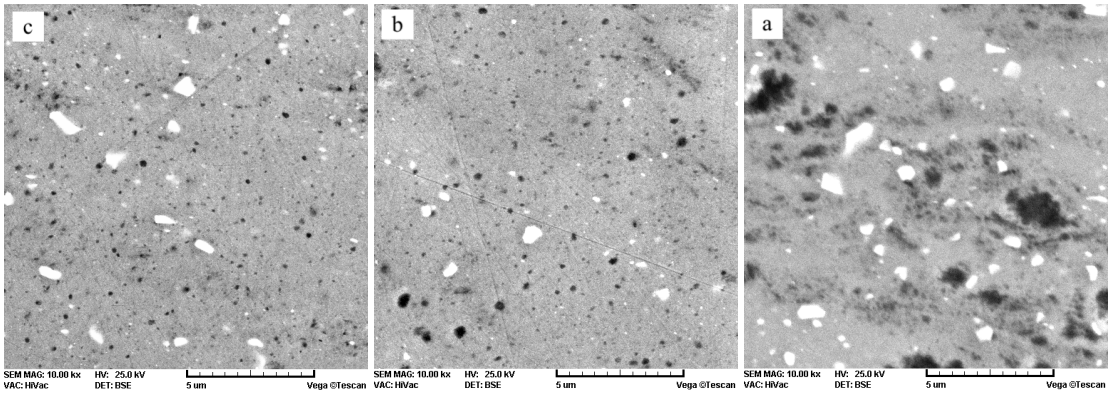

Fig. 7- SEM images of distribution of Al_2O_3 particles in surface composite layers at rotation speed of 1000 rpm and travel speed of 135 mm/min with a) one pass b) two passes, and c) three passes of FSP.

3.2.1. Distribution of reinforcing particles

Fig. 6 shows typical SEM images of stirred zone illustrating the distribution of reinforcements in surface composite layers after single pass of FSP with rotation speed of 1000 rpm and travel speeds of 135 mm/min and 330 mm/min. In these images, dark spots represent the Al_2O_3 particles and the light ones represent the precipitation of initial Al alloy. As it can be seen, at constant ω the increase in ν from 135 to 330 mm/min led to agglomeration of ceramic particles and consequently diminished their distribution. To clarify it more, decreasing in the ω/ν ratio led to reduction in numbers of rotations per millimeter and caused an increment in material flow. Yet, it can be stated that regardless of the values of ω and ν, distribution of Al_2O_3 particles in the Al matrix in none of the fabricated samples with single FSP pass is completely uniform. Distribution of Al_2O_3 particles in stirred zone became more uniform with an increase in number of passes, which is obvious in Fig. 7 as well. As it can be observed after three FSP passes, distribution

of Al_2O_3 nano particles became reasonably uniform and there are barely agglomerated Al_2O_3 nano particles with diameter of 500 nm. After four passes, Al_2O_3 nano particles with diameter of 50 nm are separated from each other as well or ultimately, two or three particles are accumulated together. This phenomenon is illustrated in Fig. 8.

3.2.2. Matrix grain size

Regarding that matrix grain sizes vary within the stir zone, they were measured from photographs of central region of stir zone, where the temperature recording and calculation of strain rates were performed. As shown in Fig. 9, with increasing ω/ν, mean grain size of surface composite layers increased, which is attributed to higher heat input and consequently higher peak temperature. Also, same trend can be observed in

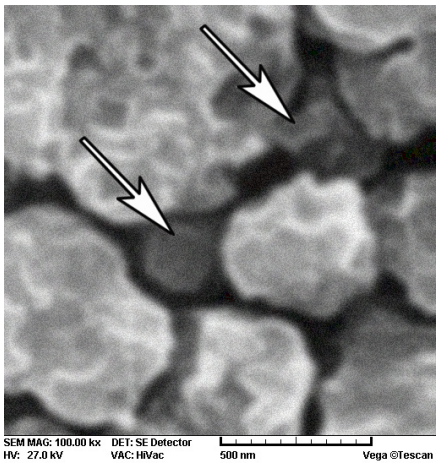

Fig. 8- SEM images of cross section of surface composite layers created with four FSP passes at rotation speed of 1600 rpm and travel speed of 135 mm/min; two alumina particles are showed with arrows.

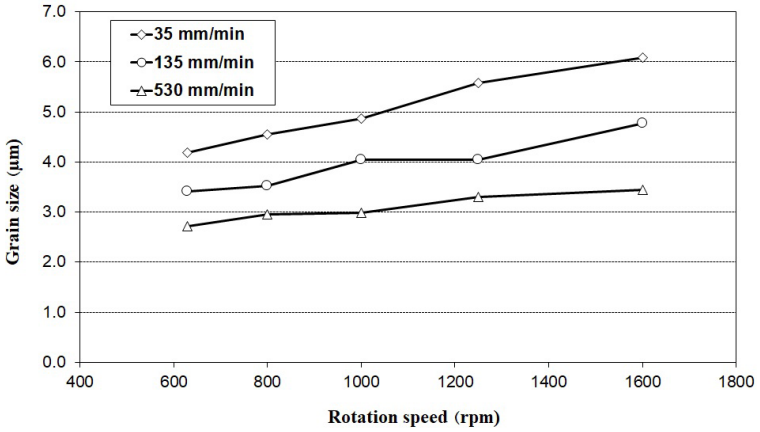

Fig. 9- Variation of grain size by rotation speed at different travel speed for surface composite layers created with one pass of FSP.

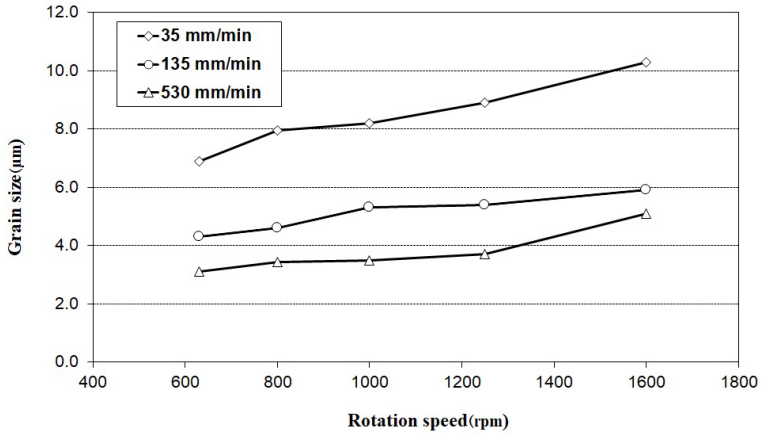

Fig. 10- Variation of grain size by rotation speed at different travel speed for surface composite layers created with one pass of FSP.

fig. 10 for FSPed samples without introducing Al_2O_3 particles. Fig. 11 shows the average grain size of Al matrix in different specimens that have undergone different numbers of passes. Several points can be concluded from this columnar chart; first, in both surface composite layers and FSPed specimens, with increasing numbers of passes, grain size decreased. Second, matrix grain size of surface composite layers are smaller than those of FSPed samples with same processing parameters. The reason is that presentation of Al_2O_3 nano particles prevented the growth of dynamic recrystallized grains, which formed due to severe plastic deformation. Third, the difference between grain size of surface composite layers and FSPed specimens arises with increasing in number of passes. In this case, it can be stated that more FSP passes contributed to dispersion of Al_2O_3 nano particles. As a consequent, the role of reinforcements in pinning grain boundaries and preventing the growth of dynamic recrystallized grains became more prominent. For instance, grain structure of surface composite layers fabricated at rotation speed of 630 rpm and travel speed 530 mm/min with 3 and 4 passes are respectively shown in Fig. 12(a) and 12(b). The average grain size of these two samples are 120 nm and 50 nm, respectively. Other average grain sizes of Al matrix are shown in Table 3 at various parameters.

3.3. Relationship between Zener-Hollomon parameter and grain size

Since FSP/FSW is a thermomechanical process, the evoluted microstructure depends on thermomechanical variables such as strain, strain rate, and temperature. This section examines the relationship between grain size and Zener-Hollomon parameter, which is characteristic of every thermomechanical process and defines as below [9]:

$$Z = \dot{\varepsilon}\exp(\frac{Q}{RT}) \quad (5)$$

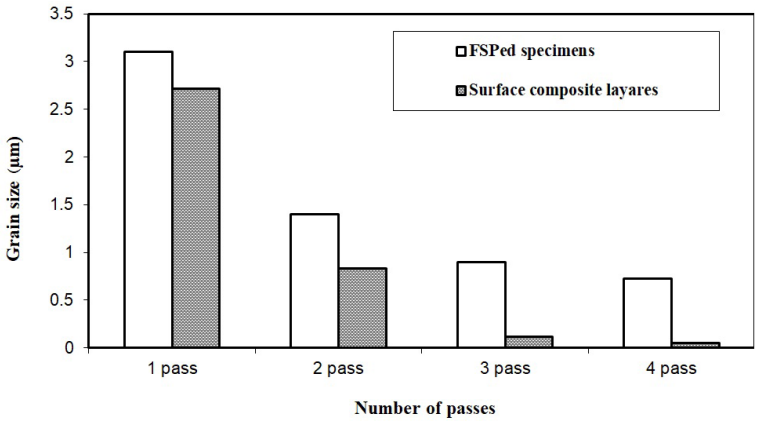

Fig. 11- Grain size of aluminum matrix for FSPed samples at rotation speed of 630 rpm and travel speed of 530 mm/min by number of passes.

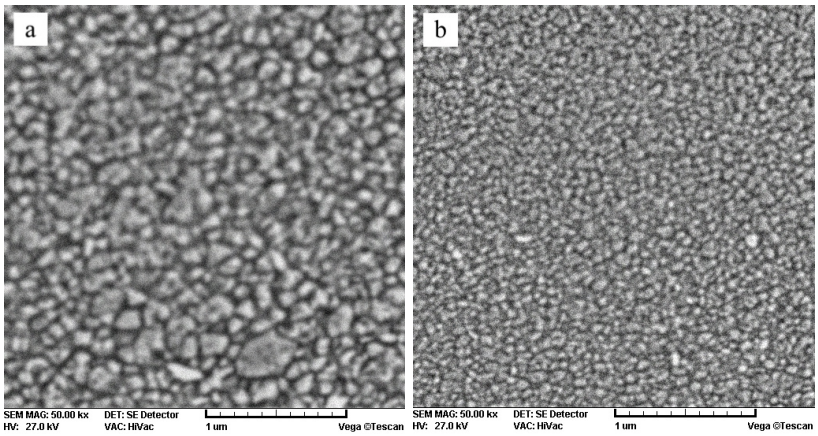

Fig. 12- High resolution SEM images of surface composite layers at rotation speed of 630 rpm and 530 mm/min with a) three and b) four passes of FSP.

Table 3- Average grain size of aluminum matrix of surface composite layers at different parameters

Rotational speed (rpm)	Travel speed (mm/min)	1 pass	2 pass	3 pass	4 pass
630	35	4.2	2.3	0.9	0.7
	135	3.4	1.4	0.4	0.3
	530	2.7	0.8	0.12	0.05
800	35	4.6	-	-	-
	135	3.5	-	-	-
	530	3.0	-	-	-
1000	35	4.9	2.5	1.0	1.0
	135	4.0	1.7	0.7	0.5
	530	3.0	1.0	0.3	0.16
1250	35	5.6	-	-	-
	135	4.0	-	-	-
	530	3.3	-	-	-
1600	35	6.1	3.1	1.6	1.2
	135	4.8	2.5	0.9	0.7
	530	3.5	1.3	0.4	0.3

Where $\dot{\varepsilon}$ is the strain rate, T is the process temperature, Q is the activation energy and R is the gas constant. The value of Q for Al is 142 kJ/mol. In FSP, both strain rate and temperature are dependents of rotation and travelling speed. For calculation of strain rate, the material flow rate must be obtained, which is due to tool's rotation motion. Therefore, the flow rate of material is equal or less than tool's rotation speed. With a simple linear estimation, the material flow rate (R_m) can be considered equal to half of the tool's rotation speed. With this estimation, strain rate during FSP can be calculated from the equation of torsional deformation, as below:

$$\dot{\varepsilon} = \frac{R_m \times 2\pi_{re}}{L_e} \quad (6)$$

Where r_e and L_e are average effective radius and depth of stirred zone, respectively. Since cross section of stirred zone is elliptical, average radius and depth are obtained by the product of in maximum visible radius and depth, respectively. According to Eq. 2; the strain rate is also expected to increase as rotation speed increases. Whereas, strain rate is not much dependent on changes travelling speed changes. The minimum and maximum values of calculated strain rate from Eq. 2 are 22.67 s^{-1} and 63.71 s^{-1}, respectively. With placing the values of strain rate and temperature in Eq. 5, Z parameter values are obtained under different variables. From Fig. 13, it is clear that at constant travelling speed the values of Z parameter decrease with increasing rotation speed.

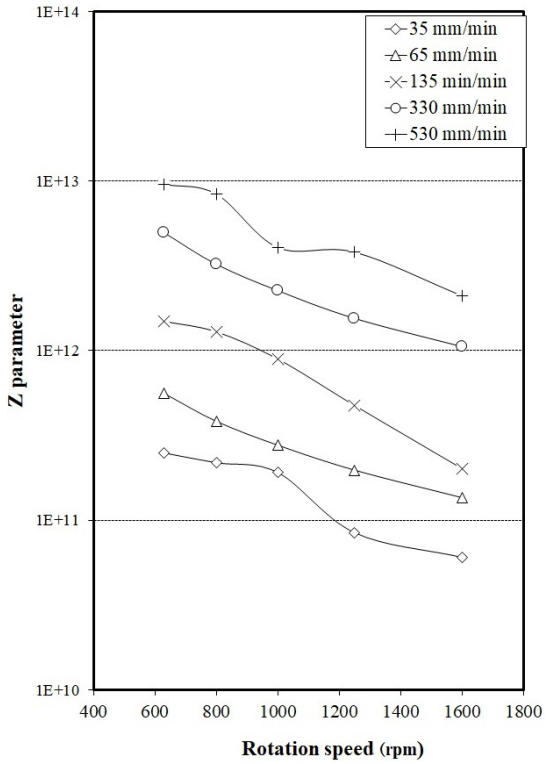

Fig. 13- Values of Z parameter by rotation speed at various travel speed.

It is noteworthy that according to Eq. 6, with increasing rotation speed, the value of strain rate increases and consequently, the value of Z parameter increases according to Eq. 5. However, on the other hand, at constant travelling speed, temperature increases by increasing rotation speed and resulting from Eq. 5 the Z parameter decreases.

Ultimately, compromising of these two factors leads to reducing the Z parameter (Fig. 13). On the effect of travelling speed on the value of Z parameter, it can be stated that according to Fig. 13, at constant rotation speed, as travelling speed increases, the temperature goes up, and subsequently, according to Eq. 5 the value of Z parameter increases. It worth noting that, the reason is that travelling speed had no significant effect on strain rate. The relationship between grain size and Zener-Hollomon parameter of Al alloys after thermomechanical operation can be defined as below:

$$d^{-1} = \mathrm{a} + \mathrm{bLn}(Z) \quad (7)$$

Where a and b are constant values and d is grain size (μm). As it is depicted in Fig. 14; the grain size decreases as the value of the Z parameter increases.

Noteworthy point about the diagram of Fig. 14 is that at specified Z parameter, there are different grain size values relevant to each number of passes. Therefore, for both surface composite layers and FSPed specimens, a particular equation should be derived for each number of passes to demonstrate the relationship between grain size and Z parameter, which are given in Table 4.

By using these equations and process variables, we can predict grain size of surface composite layers or FSPed specimens. It is also observed in Fig. 14 that at specified Z parameter, with increasing numbers of passes, the difference between grain size of each pass and its previous pass decreased. This trend is more obvious in surface composite layers in comparison with FSPed specimens, which is attributed to the presence of Al_2O_3 nano particles. In fact, increasing the number of passes in case

Table 4- Relation between grain size and Z parameter for surface composite layers and FSPed specimens

Relation between grain size and Z parameter		Number of passes
FSPed specimens	Surface composite layers	
d^{-1} = 0.0434Ln(Z) - 0.9939	d^{-1} = 0.0365Ln(Z) - 0.7369	1 pass
d^{-1} = 0.1063Ln(Z) - 2.5338	d^{-1} = 0.1655Ln(Z) - 3.8944	2 pass
d^{-1} = 0.1602Ln(Z) - 3.7844	d^{-1} = 1.0244Ln(Z) - 25.725	3 pass
d^{-1} = 0.1998Ln(Z) - 4.76139	d^{-1} = 2.353Ln(Z) - 60.359	4 pass

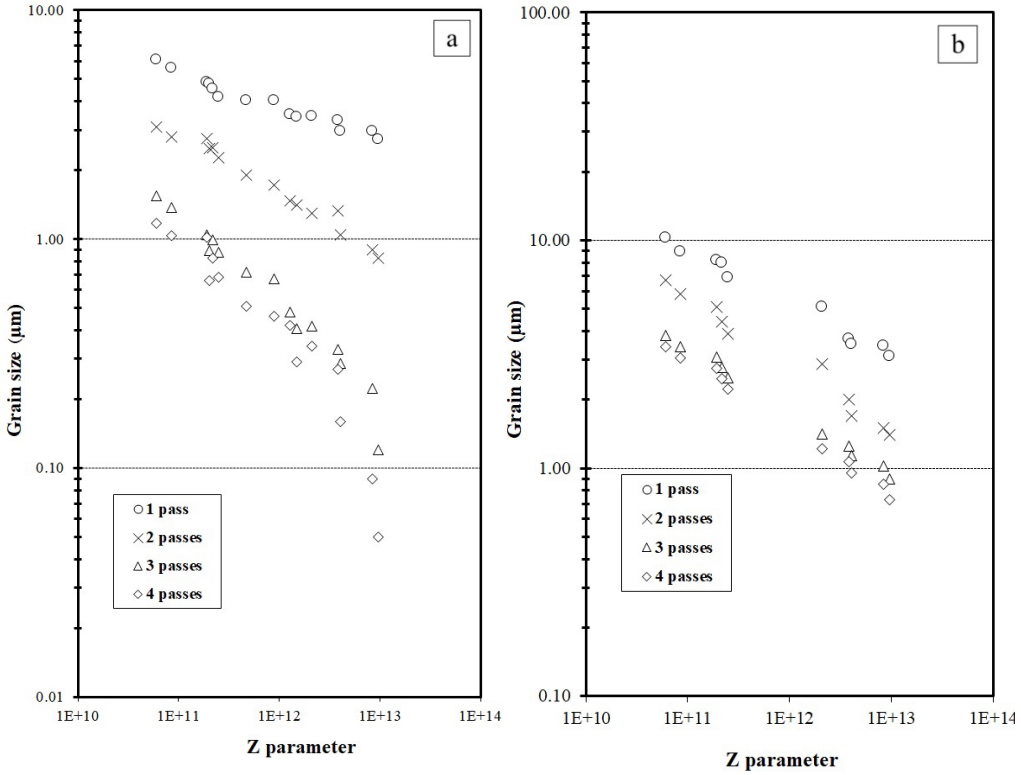

Fig. 14- Relation between grain size and Z parameter at different passes for a) surface composite layers and b) FSPed specimens.

of surface composite layers played two rules; it contributes to both more dynamic recrystallization owing to more plastic deformation and more uniform distribution of Al_2O_3 particle. Therefore, it can enhance the impact of reinforcements on grain refinement. On the other hand, in the case of FSPed specimens, increasing the number of passes just causes to increase the plastic deformation.

4. Conclusions

The processing window besides the status of created imperfections in Al-Al_2O_3 surface nano composite layers fabricated by FSP were obtained. In addition, a simple model based on Z parameter for predicting the average grain size of the matrix has been developed. It was found that presentation of Al_2O_3 nano particles could obstruct the grain growth of matrix after dynamic recrystallization. Findings indicated that more FSP passes could intensify the impact of reinforcements particles in pinning grain boundaries. Comparison of matrix grain sizes in nano-composites with those of FSPed samples without reinforcement has been indicated that increasing in number of passes leads to more grain refinement not only by repeating dynamic recrystallization but also by distribution of particles more uniformly. Here in fact, the presented model has been stablished a relationship between microstructural aspects and processing parameters for Al based composites. This model could be employed with caution in any severe plastic deformation process where predictions of outcomes are needed. Future works should entail developing this model for other metal-based composites fabricated by FSP.

References

1. Luo X, Yao Z, Zhang P, Gu D. Al2O3 nanoparticles reinforced Fe-Al laser cladding coatings with enhanced mechanical properties. Journal of Alloys and Compounds. 2018;755:41-54.
2. Visakh PM, Nazarenko OB, Sarath Chandran C, Melnikova TV, Nazarenko SY, Kim JC. Effect of electron beam irradiation on thermal and mechanical properties of aluminum based epoxy composites. Radiation Physics and Chemistry. 2017;136:17-22.
3. Harshavardhan K, Nagendran S, Shanmugasundaram A, Pravin Sankar SR, Sai Kowshik K. Investigating the effect of reinforcing SiC and graphite on aluminium alloy brake rotor using plasma spray process. Materials Today: Proceedings. 2021;38:2706-12.
4. Narimani M, Lotfi B, Sadeghian Z. Investigating the microstructure and mechanical properties of Al-TiB2 composite fabricated by Friction Stir Processing (FSP). Materials Science and Engineering: A. 2016;673:436-42.
5. Shafiei-Zarghani A, Kashani-Bozorg SF, Zarei-Hanzaki A. Microstructures and mechanical properties of Al/Al2O3 surface nano-composite layer produced by friction stir processing. Materials Science and Engineering: A. 2009;500(1-2):84-91.
6. Shafiei-Zarghani A, Kashani-Bozorg SF, Hanzaki AZ. Wear assessment of Al/Al2O3 nano-composite surface layer produced using friction stir processing. Wear. 2011;270(5-6):403-12.
7. Bourkhani RD, Eivani AR, Nateghi HR. Through-thickness inhomogeneity in microstructure and tensile properties and tribological performance of friction stir processed AA1050-Al2O3 nanocomposite. Composites Part B: Engineering. 2019;174:107061.
8. Qin D, Shen H, Shen Z, Chen H, Fu L. Manufacture of biodegradable magnesium alloy by high speed friction stir processing. Journal of Manufacturing Processes. 2018;36:22-32.
9. Ardell AJ. Precipitation hardening. Metallurgical Transactions A. 1985;16(12):2131-65.
10. Rajeshkumar R, Udhayabanu V, Srinivasan A, Ravi KR. Microstructural evolution in ultrafine grained Al-Graphite composite synthesized via combined use of ultrasonic treatment and friction stir processing. Journal of Alloys and Compounds. 2017;726:358-66.
11. You GL, Ho NJ, Kao PW. In-situ formation of Al2O3 nanoparticles during friction stir processing of AlSiO2 composite. Materials Characterization. 2013;80:1-8.
12. Moghaddam M, Zarei-Hanzaki A, Pishbin MH, Shafieizad AH, Oliveira VB. Characterization of the microstructure, texture and mechanical properties of 7075 aluminum alloy in early stage of severe plastic deformation. Materials Characterization. 2016;119:137-47.
13. Lapin J, Štamborská M, Pelachová T, Čegan T, Volodarskaja A. Hot deformation behaviour and microstructure evolution of TiAl-based alloy reinforced with carbide particles. Intermetallics. 2020;127:106962.
14. Jain VKS, Yazar KU, Muthukumaran S. Development and characterization of Al5083-CNTs/SiC composites via friction stir processing. Journal of Alloys and Compounds. 2019;798:82-92.
15. Razmpoosh MH, Zarei-Hanzaki A, Imandoust A. Effect of the Zener–Hollomon parameter on the microstructure evolution of dual phase TWIP steel subjected to friction stir processing. Materials Science and Engineering: A. 2015;638:15-9.
16. Abbasi-Baharanchi M, Karimzadeh F, Enayati MH. Effects of Friction Stir Process Parameters on Microstructure and Mechanical Properties of Aluminum Powder Metallurgy Parts. Journal of Advanced Materials and Processing. 2016 Mar 1;4(1):38-55.
17. Selvam K, Prakash A, Grewal HS, Arora HS. Structural refinement in austenitic stainless steel by submerged friction stir processing. Materials Chemistry and Physics. 2017;197:200-7.
18. Xu N, Feng R-N, Guo W-F, Song Q-N, Bao Y-F. Effect of Zener–Hollomon Parameter on Microstructure and Mechanical Properties of Copper Subjected to Friction Stir Welding. Acta Metallurgica Sinica (English Letters). 2019;33(2):319-26.
19. Ammouri AH, Kheireddine AH, Hamade RF. A Numerical Model for Predicting the Zener-Hollomon Parameter in the Friction Stir Processing of AZ31B. Materials Science Forum. 2014;783-786:93-9.
20. Chang CI, Lee CJ, Huang JC. Relationship between grain size and Zener–Holloman parameter during friction stir processing in AZ31 Mg alloys. Scripta Materialia. 2004;51(6):509-14.
21. Frigaard , Grong , Midling OT. A process model for friction stir welding of age hardening aluminum alloys. Metallurgical and Materials Transactions A. 2001;32(5):1189-200.